ORIGINAL PAPER

CrossMark

Prediction of brain deformations and risk of traumatic brain injury due to closed-head impact: quantitative analysis of the effects of boundary conditions and brain tissue constitutive model

Fang Wang[1,2] · **Yong Han[1,2]** · **Bingyu Wang[1,2]** · **Qian Peng[1,2]** · **Xiaoqun Huang[1,2]** · **Karol Miller[3,4]** · **Adam Wittek[3]**

Abstract

In this study, we investigate the effects of modelling choices for the brain–skull interface (layers of tissues between the brain and skull that determine boundary conditions for the brain) and the constitutive model of brain parenchyma on the brain responses under violent impact as predicted using computational biomechanics model. We used the head/brain model from Total HUman Model for Safety (THUMS)—extensively validated finite element model of the human body that has been applied in numerous injury biomechanics studies. The computations were conducted using a well-established nonlinear explicit dynamics finite element code LS-DYNA. We employed four approaches for modelling the brain–skull interface and four constitutive models for the brain tissue in the numerical simulations of the experiments on post-mortem human subjects exposed to violent impacts reported in the literature. The brain–skull interface models included direct representation of the brain meninges and cerebrospinal fluid, outer brain surface rigidly attached to the skull, frictionless sliding contact between the brain and skull, and a layer of spring-type cohesive elements between the brain and skull. We considered Ogden hyperviscoelastic, Mooney–Rivlin hyperviscoelastic, neo–Hookean hyperviscoelastic and linear viscoelastic constitutive models of the brain tissue. Our study indicates that the predicted deformations within the brain and related brain injury criteria are strongly affected by both the approach of modelling the brain–skull interface and the constitutive model of the brain parenchyma tissues. The results suggest that accurate prediction of deformations within the brain and risk of brain injury due to violent impact using computational biomechanics models may require representation of the meninges and subarachnoidal space with cerebrospinal fluid in the model and application of hyperviscoelastic (preferably Ogden-type) constitutive model for the brain tissue.

Keywords Brain–skull interface · Brain injury · Brain tissue constitutive model · Computational biomechanics of the brain

1 Introduction

Around 10 million people world-wide suffer from traumatic brain injury (TBI) every year (Fahlstedt et al. 2016). Given the associated risk of death and need for hospitalisation, TBI has been recognised as a significant public health and socio-economic problem (Almeida et al. 2016; Peeters et al. 2015). TBI induced by vehicular accidents is one of the major causes of mortality and permanent disability in many countries (Faul et al. 2010). For instance, in the USA, such accidents account for the greatest fraction (31.8%) of the TBI-related deaths (Faul et al. 2010).

Extensive research effort has been directed to understand the TBI mechanisms and design various countermeasures to prevent TBI. This includes experimental (Agrawal et al. 2015; Feng et al. 2010; Hardy 2007; Hardy et al. 2001; Miller and Chinzei 2002; Miller et al. 2000; Rashid et al. 2013) as well as computational biomechanics studies that are typically conducted using head/brain models implemented by means of finite element method (Kleiven and Hardy 2002; Mao et al. 2013; Miller 2011; Miller et al.

✉ Fang Wang
wangfang@xmut.edu.cn

1 School of Mechanical and Automotive Engineering, Xiamen University of Technology, Xiamen 361024, China

2 Fujian Collaborative Innovation Center for R&D of Coach and Special Vehicle, Xiamen 361024, China

3 Intelligent System for Medicine Laboratory, The University of Western Australia, Perth, WA 6009, Australia

4 Institute of Mechanics and Advanced Materials, Cardiff School of Engineering, Cardiff University, Wales, UK

2010; Yang et al. 2008; Yang and King 2011; Zhang et al 2001). There are appreciable differences between these models including constitutive modelling of the brain tissue and representation of boundary conditions of the brain.

The constitutive behaviour of the brain tissue has been a subject of substantial experimental research effort (Bilston 2011; Miller 2011; Miller and Chinzei 2002; Miller et al. 2000, 2011; Rashid et al. 2013). Although there is no consensus of what specific constitutive model should be used, there is overwhelming experimental evidence that the brain tissue exhibits nonlinear stress–strain relationship that can be accurately represented using hyperelastic/hyperviscoelastic constitutive models (Miller 2011; Miller and Chinzei 2002; Miller et al. 2000). Investigation of boundary conditions for the brain and other organs attracted much less attention of the biomechanics research community than tissue constitutive behaviour (Wittek et al. 2016). However, the importance of representation of boundary conditions in computational biomechanics models of the brain has been confirmed in several studies (Bayly et al. 2012; Kleiven and Hardy 2002; Wittek and Omori 2003).

Boundary conditions of the brain are determined by the brain–skull interface that consists of several layers of tissues located between the brain and skull (Fig. 1). While the constitutive properties of some of these layers have been investigated (Jin 2009; Jin et al. 2011, 2014), the exact anatomical structure of the brain–skull interface remains a subject of debate (Haines et al. 1993) and there is little quantitative information about the interactions between the tissue layers within the brain–skull interface (Wittek et al. 2016). This makes problematic any attempts to model the brain–skull interface by directly representing the interface anatomical structure. Therefore, a number of simplified approaches for modelling of the brain–skull interface were proposed and used. By comparing stress/strain within the pig brain obtained using a 2-D computational biomechanics model and from the experiments using pigs, Miller et al. (1998) found that a sliding contact algorithm was suitable to predict the location and distribution of axonal injury. This approach was also recommended in the modelling study by Al-Bsharat et al. (1999). Similarly, Agrawal et al. (2015), from the experimental and computational modelling studies of samples consisting of the skull, brain–skull interface and brain tissue, suggested a frictionless contact as the most suitable approach for modelling interactions between the brain and skull under compression at low loading speeds. Zhang et al (2001) selected sliding contact allowing no separation to represent the brain–skull interface. In contrast, Claessens et al. (1997) suggested that a no-slip interface, allowing no movement between the brain surface and skull, results in a better agreement with the experiments than sliding contact. Kleiven and Hardy (2002) and
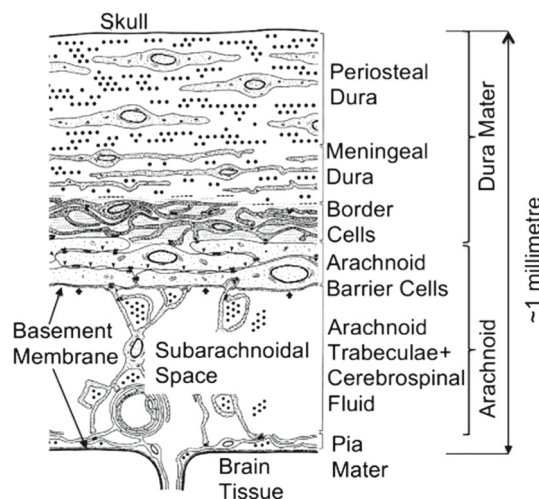

Fig. 1 Anatomical structures of brain–skull interface. Modified from Haines et al. (1993)

Wittek and Omori (2003) suggested that for accurate modelling of the brain–skull interface, direct representation of the subarachnoidal space/cerebrospinal fluid as a water-like medium is needed. This approach has been also used in the head/brain model developed by Yang (2011), Total HUman Model for Safety (THUMS) by Toyota Motor Corporation and Toyota Central R&D Labs (Shigeta et al. 2009; Watanabe et al. 2011), the models developed at Wayne State University (Mao et al. 2006; Zhang et al 2001), and Simulated Injury Monitor (SIMon) model (Takhounts et al. 2013).

As none of the currently used approaches for modelling the brain–skull interface in computational biomechanics models for prediction of the brain responses due to surgery and/or violent impact has been widely accepted and no consensus regarding the specific type of constitutive model for the brain tissue exists, there is an urgent need to quantify the effects of assumptions and simplifications when modelling the brain–skull interface and selecting the constitutive model for the brain tissue on predicting the brain deformations and risk of traumatic brain injury due to transient loads. Such need was confirmed by our recent study (Wang et al. 2017) in which we investigated these effects for a single impact pulse acting on a post-mortem human subject and linear elastic and Ogden-type constitutive models for the brain tissue. While building on the experience gained from Wang et al. (2017), in the current study we significantly expand the investigation scope by conducting the analysis for different impact locations (frontal and occipital), different impact pulses, different types of hyperelastic constitutive models for the brain tissue, and investigating the effects on not only the brain tissue deformations but also on the selected traumatic brain injury criteria.

2 Materials and methods

2.1 Model description

The purpose of the current study is to quantify the effects of assumptions and simplifications regarding boundary conditions for the brain and constitutive model of the brain tissue on prediction of the brain deformations and traumatic brain injury risk due to violent impact rather than creating a new model of the brain. Therefore, following Wang et al. (2017), we used the previously validated head/brain model extracted from well-established THUMS Version 4.0 human body model by Toyota (Shigeta et al. 2009; Watanabe et al. 2011) implemented using the LS-DYNA explicit dynamics nonlinear finite element code (LSTC 2007) (Fig. 2a, b). The THUMS brain model includes representation of key tissues and anatomical components of the brain: grey matter, white matter, falx, subarachnoidal cerebrospinal fluid (CSF), dura, arachnoid and pia (Fig. 2c), consisting of a total of over 31,000 elements and 24,800 nodes. The skull and brain parenchyma are discretised using under-integrated 8-noded hexahedral elements, while dura, arachnoid and pia mater are represented using layers of 4-noded shell elements. Tied contact interfaces that allow no sliding and separation are defined between the skull inner surface and dura mater, and between dura mater and arachnoid. The subarachnoidal CSF is represented using a layer of 8-noded hexahedral elements with water-like material properties (Fig. 2d).

Investigation of the effects of approach for modelling the boundary conditions of the brain and constitutive model of the brain tissue was carried out by modelling the experiments on the head-neck complexes of post-mortem human subjects (PMHSs) conducted by Hardy et al. (2001). The study by Hardy et al. (2001) was selected as it contains quantitative information about the experimentally determined displacements at 12 locations within the PMHSs' brains. We used six experiments [experimental series C383 and C755 in Hardy et al. (2001)] conducted using two PMHSs (i.e. three experiments for each PMHS). They represent different impact location (frontal and occipital), but exhibit similar impact severity (as measured by the peak angular speed of the head), for a given location and subject. Therefore, they provide some insight into intra-subject variation of the biomechanical responses. Detailed information is in Table 1.

Following the experiments by Hardy et al. (2001), the entire cervical spine together with the head/brain from the THUMS Version 4.0 model was included in the model used in this study. The first (T1) and second (T2) thoracic vertebrae, scapula, collar bones and sternum were fully (rigidly) constrained to form a base for the cervical spine (Fig. 2b).

The load was defined, by prescribing the head angular speed–time histories (around all three axes of the coordinate system associated with the head COG as defined in Fig. 3) reported by Hardy et al. (2001).

All simulations in this study were conducted using the LS-DYNA 971 nonlinear explicit finite element code by Liv-
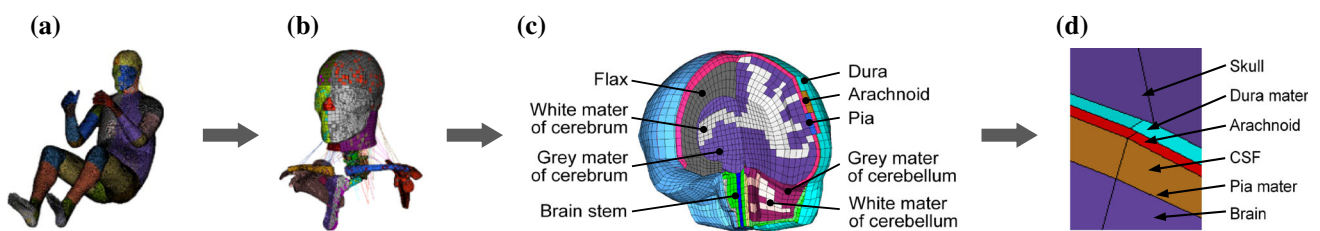

Fig. 2 **a** THUMS version 4.0 model in sitting posture; **b** isolated head-neck complex of THUMS version 4.0 model used in this study. The first (T1) and second (T2) thoracic vertebrae, scapula, collar bones and sternum were fully constrained to provide a base for the cervical spine; **c** THUMS version 4.0 brain model; **d** brain–skull interface representation in THUMS Version 4.0 brain model, adapted from our recent paper (Wang et al. 2017)

Table 1 Impact pulses from Hardy et al. (2001) and their major characteristics used in the current study

Post-mortem human subject	Test	Impact location	Peak angular speed (forward flexion, rad/s)	$HIC_{15\,ms}$
C383	C383-T1	Frontal	4/− 20	47
	C383-T2	Frontal	2/− 22	34
	C383-T3	Frontal	4/− 22	68
C755	C755-T2	Occipital	18/− 1	17
	C755-T3	Occipital	19/− 2	22
	C755-T4	Occipital	17/− 4	31

$HIC_{15\,ms}$ is the head injury criterion (HIC) measured over 15 ms (NHTSA 2010). It is the most commonly used criterion for evaluating the risk of head injury
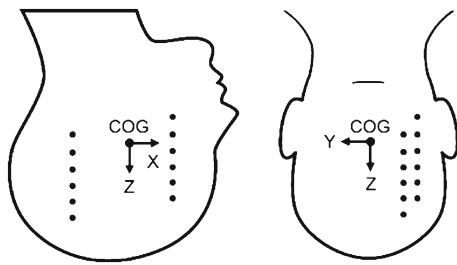
Fig. 3 Schematic representation of location of the markers (neutral density targets NDTs) implanted in the brain in the experiments by Hardy (2007) and Hardy et al. (2001). Based on Hardy et al. (2001) and adapted from our recent paper (Wang et al. 2017)

ermore Software Corporation (Livermore, CA, USA; http://www.lstc.com).

In the experiments by Hardy (2007) and Hardy et al. (2001), information about the brain deformations was obtained by X-ray tracking of the motion of twelve markers (NDTs: neutral density targets) implanted into the brain (Hardy 2007; Hardy et al. 2001) (Figs. 3, 4a). We used the trajectories, displacement–time histories and excursions of the NDTs, reported in Hardy et al. (2001), to evaluate the biofidelity of the approaches for modelling the brain–skull interface and brain tissue constitutive models analysed in this study. Following Hardy et al. (2001) and Hardy (2007), the excursions are defined as the difference between the maximum positive and negative displacements in the impact direction measured in reference to the starting (before the impact) location in the coordinate system with origin at the head COG (Fig. 3). We analysed the displacements of the selected nodes (Fig. 4b) located closely to the positions of NDTs reported by Hardy et al. (2001).

2.2 Modelling approaches for the brain–skull interface

Following our recent study (Wang et al. 2017), we analysed four approaches for modelling the brain–skull interface with varying complexity (see Table 2):

(1) The approach used in THUMS Version 4.0 brain model (Cases 1–1, 1–2, 1–3 and 1–4 in Table 2) that includes direct representation of the CSF, dura, arachnoid and pia mater. The material properties of the brain–skull interface in THUMS model (Iwamoto et al. 2015; Kimpara et al. 2006) are given in Table 3.

(2) The brain outer surface (bounded by the pia mater) rigidly attached to the skull through the LS-DYNA tied contact interface (Cases 2–1, 2–2, 2–3 and 2–4 in Table 2)—application of this approach has been reported by Claessens et al. (1997).

(3) Frictionless sliding contact between the brain and skull (Cases 3–1, 3–2, 3–3 and 3–4 in Table 2)—this approach has been successfully used in the studies on predicting the brain deformations due to craniotomy (surgical opening of the skull) by Hu (2007) and Wittek et al. (2010). It was also recommended for compressive loading in the experimental and computational study by Agrawal et al. (2015).

(4) The brain–skull interface represented with a thin layer of spring-type (no damping) cohesive elements (Cases 4–1, 4–2, 4–3 and 4–4 in Table 2)—this approach has been previously used by Feng et al. (2010) in investigation of the brain responses due to frontal impacts. However, the formulation we used here is directly based on the newer experimental study by Mazumder et al. (2013) who sug-
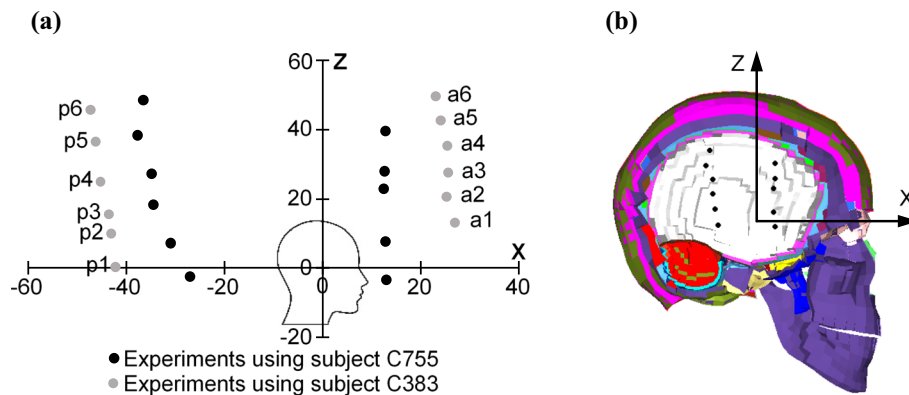

Fig. 4 a Initial position (in a coordinate system with origin at the head gravity centre COG, see Fig. 3) of the NDTs in the experiments by Hardy et al. (2001). Position of NDT #a6 marker of subject C755 is not reported in Hardy et al. (2001). X–Z coordinate system origin is at the head COG (see Fig. 3); b current study: nodes in the THUMS Version 4.0 brain model representing the NDTs for subject C755. X–Z coordinate system origin is at the head COG (see Fig. 3)

Table 2 Simulation matrix for studying the effects of approaches for modelling the brain–skull interface and brain tissue constitutive model

Brain tissue constitutive model	Modelling approach for brain–skull interface			
	Original THUMS head/brain model (see Fig. 1d)	Brain rigidly attached to the skull	Frictionless contact between the brain and skull	Cohesive layer (spring-type) between the brain and skul
Ogden hyperviscoelastic model	Case 1–1	Case 2–1	Case 3–1	Case 4–1
Linear viscoelastic model	Case 1–2	Case 2–2	Case 3–2	Case 4–2
Mooney–Rivlin hyperelastic model	Case 1–3	Case 2–3	Case 3–3	Case 4-3
neo-Hookean hyperelastic model	Case 1-4	Case 2-4	Case 3-4	Case 4–4

Table 3 Material properties used in the brain–skull interface in THUMS model

Part	Mass density (kg/m^3)	Young's modulus (MPa)	Poisson ratio	Thickness (mm)
CSF	1000	1.6E−4	0.49	
Pia mater	1000	1.1	0.40	0.4
Arachnoid	1000	1.1	0.40	0.4
Dura mater	1133	70	0.45	1

gested linear springs with stiffness of 11.45 Nm^{-1}/mm^2, rather than the contact interfaces, as the most appropriate approach for modelling the brain–skull interface.

Given the anatomical structure of the brain–skull interface (Fig. 1), Case 2–1 (brain surface rigidly attached to the skull) and Case 3–1 (frictionless contact that allows for free sliding and separation between the brain and skull) can be regarded as two extreme modelling approaches. It might be expected that the actual behaviour of the brain–skull interface would fall between them.

2.3 Constitutive models and properties of the brain tissue

In the THUMS Version 4.0 brain model and many other computational biomechanics human body models used in injury analysis and prevention (Takhounts et al. 2013; Yang 2011; Zhang et al 2001), the brain parenchyma is modelled using a linear viscoelastic constitutive model. However, numerous experimental studies have indicated that the brain tissue exhibits the behaviour that is best represented using hyperelastic or hyperviscoelastic constitutive models (Miller and Chinzei 1997, 2002; Wittek et al. 2008).

In this study, detailed analysis of the predicted deformations and strains within the brain has been conducted for Ogden hyperviscoelastic model (Cases 1–1, 2–1, 3–1 and

4–1 in Table 2). This model accounts for the difference between the tensile and compressive stiffness of the brain tissue (Miller and Chinzei 2002) and different shapes of stress–strain relationship (defined by the material coefficient α, see Eq. 1 below):

$$W = \frac{2}{\alpha^2} \int_0^t \left[G(t - \tau) \frac{d}{d\tau} \left(\lambda_1^\alpha + \lambda_2^\alpha + \lambda_3^\alpha - 3 \right) \right] d\tau + K(J - 1 - \ln J) \tag{1}$$

$$G(t) = G_i + (G_0 - G_i)e^{\frac{-t}{\tau}} \tag{2}$$

where W is the potential function, λ_i ($i = 1, 2, 3$) is the principal stretch, G_0 is an instantaneous shear modulus, G_i is the relaxed shear modulus, τ is the characteristic time, α is the material coefficient which can assume any real value without restrictions (Wittek et al. 2007), K is the bulk modulus, and J is the relative volume change.

Ogden model has been found by Miller and Chinzei (2002) and Mihai et al. (2015) to provide an excellent agreement with the brain tissue behaviour, and the deficiency of simpler neo-Hookean (Ogden 1997) and Mooney–Rivlin (Rashid et al. 2013) (Eqs. 3, 4 below) models was highlighted by Mihai et al. (2015). However, Takhounts et al. (2003) reported that the Ogden and Mooney–Rivlin models yield similar results when predicting the brain responses under impacts. Therefore, our analysis includes also neo-Hookean (Case 1–3) and Mooney–Rivlin (Case 1–4) hyperelastic models (Table 2):

Table 4 Constitutive models and parameters for the brain tissue used in this study

Part	Linear viscoelastic model, Mooney–Rivlin hyperelastic model and neo-Hookean hyperelastic model			Ogden hyperviscoelastic model			
	G_0 (Pa)	G_i (Pa)	τ(s)	G_0(Pa)	α	G_i (Pa)	τ(s)
White matter cerebrum	1100	550	0.06	1100	− 4.7	550	0.06
White matter cerebellum	1100	550	0.06	1100	− 4.7	550	0.06
Grey matter cerebrum	850	425	0.06	850	− 4.7	425	0.06
Grey matter cerebellum	850	425	0.06	850	− 4.7	425	0.06

See Eqs. 1 and 2 for explanations of the symbols

Table 5 Definition of the brain material properties sets for the parametric study of the effects of brain tissue material properties on the brain model responses

Set	Part	Linear viscoelastic model			Ogden hyperviscoelastic model			
		G_0 (Pa)	G_i (Pa)	τ(s)	G_0 (Pa)	α	G_i (Pa)	τ(s)
Set 1	White matter cerebrum	1100	550	0.06	1100	− 4.7	550	0.06
	White matter cerebellum	1100	550	0.06	1100	− 4.7	550	0.06
	Grey matter cerebrum	850	425	0.06	850	− 4.7	425	0.06
	Grey matter cerebellum	850	425	0.06	850	− 4.7	425	0.06
Set 2	White matter cerebrum	12,500	6100	0.06	12,500	− 4.7	6100	0.06
	White matter cerebellum	12,500	6100	0.06	12,500	− 4.7	6100	0.06
	Grey matter cerebrum	10,000	5000	0.06	10,000	− 4.7	5000	0.06
	Grey matter cerebellum	10,000	5000	0.06	10,000	− 4.7	5000	0.06
Set 3	White matter cerebrum	22,200	8700	0.06	22,200	− 4.7	8700	0.06
	White matter cerebellum	22,200	8700	0.06	22,200	− 4.7	8700	0.06
	Grey matter cerebrum	18,000	7000	0.06	18,000	− 4.7	7000	0.06
	Grey matter cerebellum	18,000	7000	0.06	18,000	− 4.7	7000	0.06
Set 4	White matter cerebrum	49,000	16,000	0.06	49,000	− 4.7	16,000	0.06
	White matter cerebellum	49,000	16,000	0.06	49,000	− 4.7	16,000	0.06
	Grey matter cerebrum	39,200	12,800	0.06	39,200	− 4.7	12,800	0.06
	Grey matter cerebellum	39,200	12,800	0.06	39,200	− 4.7	12,800	0.06

See Eqs. 1 and 2 for explanations of the symbols

$$W = A \left(\lambda_1{}^2 + \lambda_2{}^2 + \lambda_3{}^2 - 3 \right)$$
$$+ B \left(\lambda_1{}^2\lambda_2{}^2 + \lambda_2{}^2\lambda_3{}^2 + \lambda_3{}^2\lambda_1{}^2 - 3 \right) \quad (3)$$
$$G_0 = 2(A + B) \quad (4)$$

where A and B are material constants. For neo-Hookean model, $A = G/2$ and $B = 0$; and for Mooney–Rivlin model, following Wittek et al. (2008), we use $A = B = G/4$, where G is the shear modulus (Table 4).

As the material properties used in THUMS brain model have been reported to be somewhat beyond the range published in the literature (Antona 2013), we used the properties (instantaneous shear modulus of 1100 Pa) that correspond to the highest strain rate applied in the experiments published by Miller and Chinzei (1997, 2002) (Table 4). As the experiments by Miller and Chinzei (1997, 2002) did not distinguish

between the properties of grey matter and white matter, we followed the assumptions used in the original THUMS Version 4.0 brain model where the white matter in the cerebrum and cerebellum was assigned a shear modulus 25% greater than the grey matter (Table 4) (Ho and Kleiven 2007; Zhang et al 2001).

Given the variation of material properties (shear modulus) of the brain tissue reported in the literature, we conducted a parametric study to investigate the effects of such variation on predicted brain deformations measured by trajectories of the NDTs (NDT #a1) located within the brain. The parametric study was conducted for four sets of material properties (Table 5) with Set 1 (the properties used when studying the effects of boundary conditions for the brain and constitutive model) treated as a base/reference:
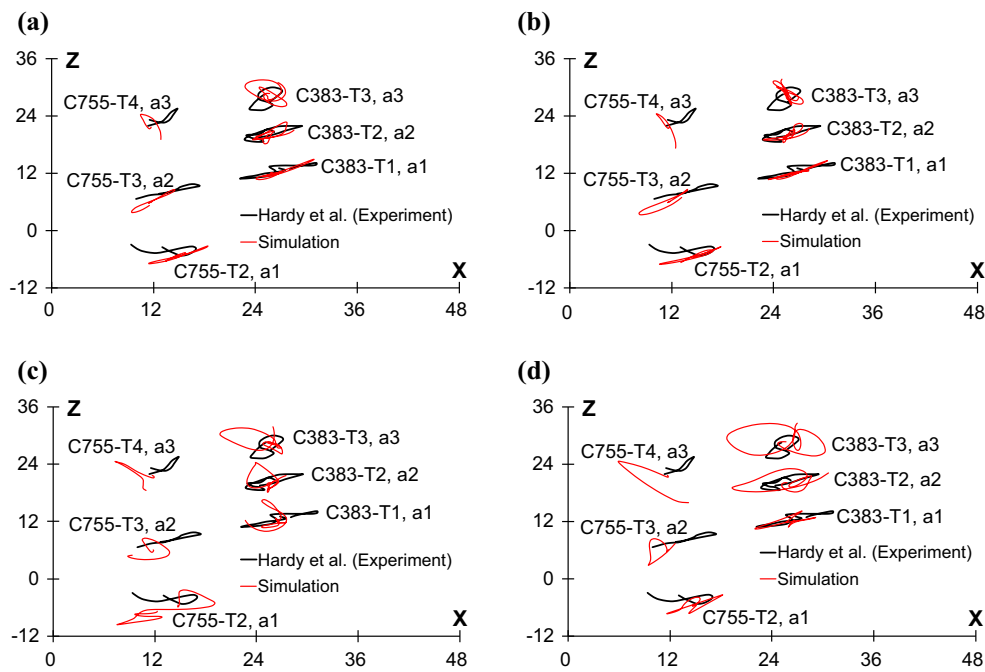
Fig. 5 Comparison of the NDT trajectories predicted using THUMS model when changing the brain–skull interface modelling approach for Ogden hyperviscoelastic model of brain tissue and experimental results by Hardy et al. (2001). The trajectories are given in the local head coordinate system (aligned with the Frankfort plane) with origin at the head COG. **a** Case 1–1: original approach used in THUMS version 4.0 model with direct representation of the CSF and brain meninges; **b** Case 2–1: brain rigidly attached to the skull; **c** Case 3–1: frictionless sliding contact between the brain and skull; **d** Case 4–1: brain–skull interface modelled using a layer of spring-type cohesive elements. The results for tests C755-T2 were reported in our previous study (Wang et al. 2017)

- *Set 1* The brain tissue material properties from the experiments by Miller and Chinzei (1997, 2002). This is the base set of the material properties used in this study. It forms the lower limit of the brain tissue shear modulus we used when investigating the effects of material properties.
- *Set 2* The brain material properties from the original THUMS Version 4.0 brain model.
- *Set 3* The brain material properties from the experiments by McElhaney et al. (1973).
- *Set 4* The brain material properties used by Antona (2015). This set forms the upper limit of the brain tissue shear modulus we use here.

We studied the effects of the brain tissue material properties only for the linear viscoelastic and Ogden hyperviscoelastic constitutive models as it may be expected that the results for the remaining constitutive models (Mooney–Rivlin and neo-Hookean) used in this study would fall within the limits formed by the linear and Ogden models. The investigation of these effects was conducted for the impact pulse C383-T3 which is the most severe load case used in this study.

2.4 Simulation matrix

In total, 120 simulations were conducted in this study (see Tables 1, 2, 5): 2 PMHSs × 3 Impact pulses × 4 Approaches for modelling the brain–skull interface × 4 Types of constitutive model + 3 Sets of material properties × 4 Approaches for modelling the brain–skull interface × 2 Selected types of constitutive model (Ogden hyperviscoelastic and linear viscoelastic). The calculations were conducted using a PC with 8-core i7 CPU (Intel Core), and each simulation took around 40 minutes.

3 Results

3.1 Effects on deformations within the brain

Analysis of the predicted trajectories of the selected markers implanted in the subject brains indicates appreciable effects of both the approach for modelling the brain–skull interface and constitutive model of the brain parenchyma (Figs. 5, 6). From the analysis of Figs. 5 and 6, it appears that the approach for the brain–skull interface modelling with direct representation of the CSF originally used in the THUMS
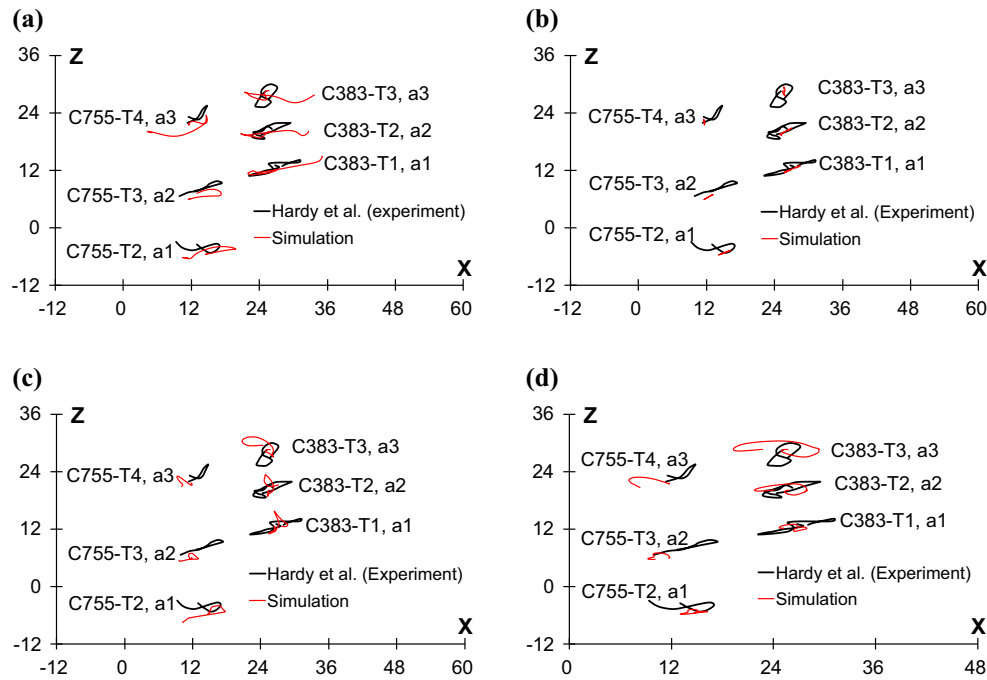
Fig. 6 Comparison of the NDT trajectories predicted using THUMS model when changing the brain–skull interface modelling approach for linear viscoelastic model of brain tissue and experimental results by Hardy et al. (2001). The trajectories are given in the local head coordinate system (aligned with the Frankfort plane) with origin at the head COG. **a** Case 1–2: original approach used in THUMS version 4.0 model with direct representation of the CSF and brain meninges; **b** Case 2–2: brain rigidly attached to the skull; **c** Case 3–2: frictionless sliding contact between the brain and skull; **d** Case 4–2: brain–skull interface modelled using a layer of spring-type cohesive elements. The results for tests C755-T2 were reported in our previous study (Wang et al. 2017)

brain model combined with Ogden hyperviscoelastic constitutive model for the brain parenchyma yields the trajectories (Fig. 5a) that are in better agreement with the experimental results by Hardy et al. (2001) than the remaining solutions we analyse here.

As injury criteria for the brain often rely on magnitude of tissue strain and strain distribution within the brain, it may be argued that the analysis should focus on the displacement magnitudes (excursions) of the selected points within the brain rather than the entire trajectories shown in Figs. 5 and 6. The experimentally obtained (Hardy et al. 2001) and predicted, using the computational biomechanics models, excursions of the selected markers within the brain when varying the constitutive model of the brain parenchyma and approach for modelling the brain–skull interface are compared in Fig. 7. For quantitative analysis of the results shown in Fig. 7, we computed the standard error σ (see Eq. 5) as a measure of difference between the experimentally obtained excursions and modelling predictions (see Table 6 for results).

$$\sigma = \sqrt{\frac{\sum E_n^2}{n}} \tag{5}$$

where E_n is the difference between experimentally obtained excursions and predictions for a given modelling case in

Fig. 7, $n = 6$ (6 experiments used in the analysis: C383-T1, C383-T2, C383-T3, C755-T2, C755-T3 and C755-T4).

The conclusions from analysis of the results shown in Fig. 7 and Table 6 are consistent with those when analysing the trajectories: the best agreement between the modelling predictions and experimental results by Hardy et al. (2001) was observed when Ogden hyperviscoelastic constitutive model was applied for the brain parenchyma (Cases 1–1, 1–2, 1–3 and 1–4) with the predicted excursions appreciably affected by the approach for modelling the brain–skull interface.

The results for approach for modelling the brain–skull interface lead to less decisive conclusions than those for constitutive model of the brain parenchyma. The predictions obtained using the approach with direct representation of the CSF taken from THUMS brain model (Cases 1–1 and 2–1) appear to exhibit the smallest differences with the experimental data by Hardy et al. (2001). For this approach, the standard error was the smallest for four out of six predicted variables characterising the markers' excursions (Table 6, Fig. 7b, c and f). However, it should be noted that for two out of six predicted variables, the approach using the brain rigidly attached to skull led to a smaller error than approach with direct representation of the CSF (Table 6, Fig. 7a, e). These results should be interpreted with caution. For three out
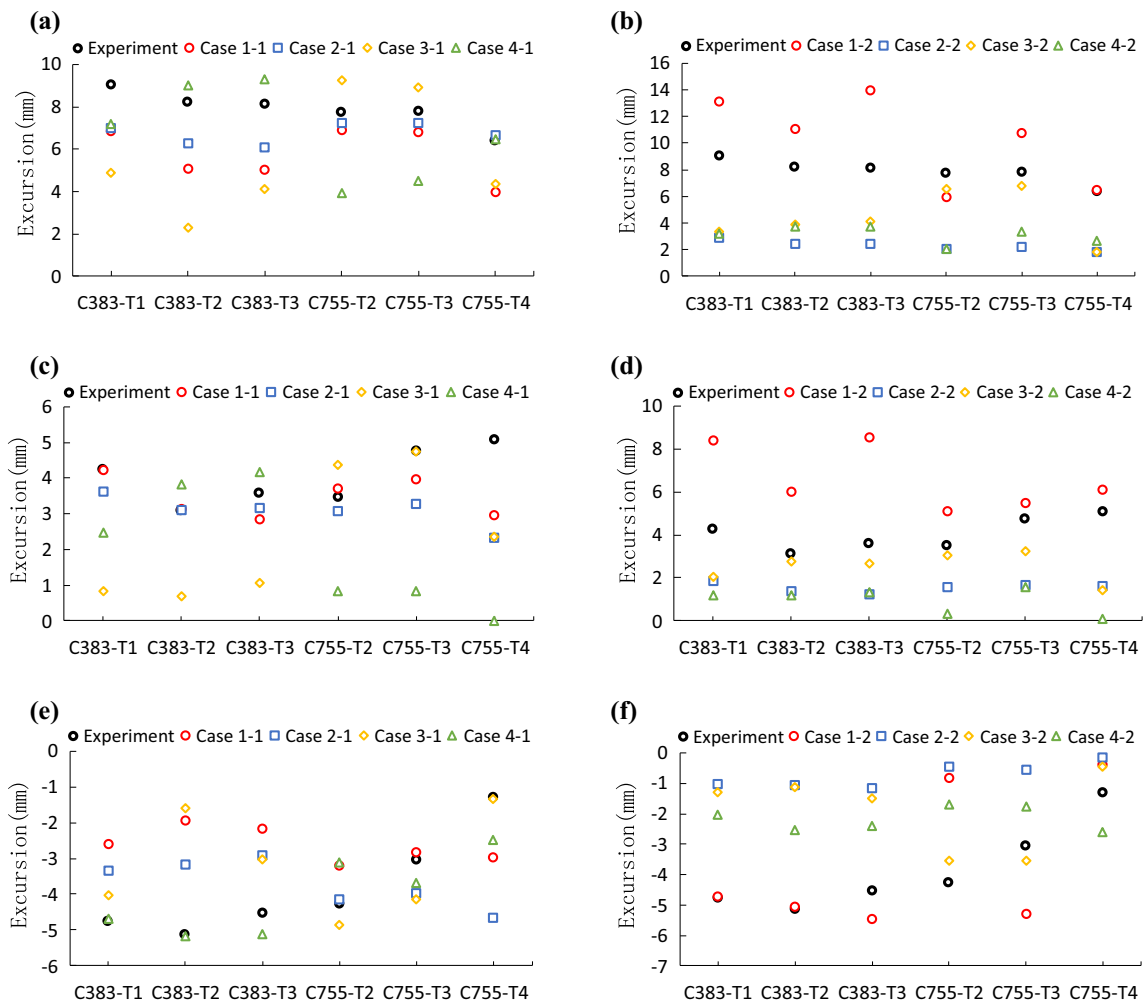
Fig. 7 Comparison of the predicted and observed [in the experiments by Hardy et al. (2001)] excursions of the selected markers (neutral density targets NDTs) located within the brain when varying the constitutive model of the brain parenchyma and approach for modelling of the brain–skull interface. The excursions are reported in the local head coordinate system with origin at the head COG. The information about the loading velocity pulses is in Table 1 and the simulation matrix in Table 2. The NDTs' location is in Fig. 4. The constitutive properties are in Table 4. With exception of experiment C755-T4 by Hardy et al. (2001), the excursions of marker NDT #a1 were analysed. For experi-

ment C755-T4, we analysed the excursions of marker NDT #a2 as no data for marker NDT #a1 were reported for this experiment by Hardy et al. (2001). **a** Total excursion magnitude using Ogden hyperviscoelastic model of the brain parenchyma; **b** total excursion magnitude using linear viscoelastic model of the brain parenchyma; **c** positive excursion using Ogden hyperviscoelastic model of the brain parenchyma; **d** positive excursion using linear viscoelastic model of the brain parenchyma; **e** negative excursion using Ogden hyperviscoelastic model of the brain parenchyma; **f** negative excursion using linear viscoelastic model of the brain parenchyma

of six predicted variables characterising the markers' excursions, the differences between the errors for the approach with direct representation of CSF taken from THUMS brain model and for the approach with the brain rigidly attached to the skull were less than 0.45 mm. This makes these errors indistinguishable for practical purposes as the standard deviation in determining the markers position in the experiments by Hardy et al. (2001) was up to 0.46 mm (Hardy 2007). Given this standard deviation, it should be also noted that for some experiments by Hardy et al. (2001) (C383-T3), application of cohesive elements to model the brain–skull interface and Ogden hyperviscoelastic model for the brain tissue (Case

4–1) resulted in closer prediction of the NDT excursions than using the remaining solutions we analyse here (Fig. 7e).

To analyse the effects of constitutive model of the brain parenchyma, we compared the displacement–time histories of marker NDT #a1 experimentally obtained by Hardy et al. (2001) with the displacement envelopes formed when varying the approach for modelling the brain–skull interface for linear viscoelastic and Ogden hyperviscoelastic constitutive models (Fig. 8). The effects are significant with a clear indication that displacement–time histories predicted using the Ogden hyperviscoelastic model are closer to the experimental results than when using linear viscoelastic model.

Table 6 The standard errors between the experimental excursions and predictions for the four cases of every sub-figure in Fig. 7

Simulation cases		Excursions		
		Total excursion	Positive excursion	Negative excursion
		Fig. 7a	Fig. 7c	Fig. 7e
Ogden hyperviscoelastic model of brain parenchyma	Case 1–1: original THUMS head/brain model (see Fig. 1d)	2.30	**0.97**	2.02
	Case 2–1: brain rigidly attached to the skull	**1.46**	1.32	1.85
	Case 3–1: frictionless Contact between the brain and skull	3.56	2.31	1.67
	Case 4–1: cohesive layer between the brain and skull	2.27	2.95	**0.77**
		Fig. 7b	Fig. 7d	Fig. 7f
Linear viscoelastic model of brain parenchyma	Case 1–2: original THUMS head/brain model (see Fig. 1d)	**3.45**	3.00	**1.77**
	Case 2–2: brain rigidly attached to the skull	5.61	2.56	3.26
	Case 3–2: frictionless contact between the brain and skull	3.87	**1.90**	2.55
	Case 4–2: cohesive layer between the brain and skull	4.82	3.24	2.19

The number in bold font indicates the smallest error (for the analysed constitutive models of the brain parenchyma and approaches for modelling the brain–skull interface) for a given variable characterising excursions of the markers implanted within the brain in the experiments by Hardy et al. (2001)

The differences between marker NDT #a1 displacement–time histories predicted using Ogden and linear constitutive models are more pronounced for subject C383 (Fig. 8a–c) than for subject C755 (Fig. 8d–f). This phenomenon can be attributed to the higher impact severity in the experiments using this subject. Consequently, the total excursions of NDT #a1 marker (and likely the associated deformations within the brain) were greater for subject C383. As differences between the Ogden and linear constitutive models are more pronounced at higher strains, one may expect more noticeable differences between the brain deformations predicted using Ogden and linear elastic model for subject C383 than for subject C755.

Other contributing factors are the impact location and associated impact pulse characteristics: frontal impact for subject C383 and occipital impact for subject C755.

The results shown in Figs. 5, 6, 7 and 8 indicate that the deformations within the brain (as measured by displacements of the selected points/NDTs) predicted when applying Ogden hyperviscoelastic model for modelling of the brain parenchyma tissues are closer to the experimental results by Hardy et al. (2001) than when linear viscoelastic model

is used. However, as stated in Materials and Methods, it has been suggested in some studies (Takhounts et al. 2003) that more simple neo-Hookean and Mooney–Rivlin models may be sufficient when predicting the brain responses under impacts. Therefore, we compared the magnitude envelopes (defined by the maximum and minimum excursion) of the predicted excursions of marker NDT #a1 located within the brain for Ogden, Mooney–Rivlin and neo-Hookean hyperviscoelastic models and the linear viscoelastic model, with the envelopes determined from the experiments by Hardy et al. (2001) (Fig. 9). The results clearly indicate that the magnitudes for Ogden hyperviscoelastic model are much closer to those observed in the experiments by Hardy et al. (2001) than for linear viscoelastic, Mooney–Rivlin and neo-Hookean models (Fig. 9).

The results reported in Figs. 5, 6, 7, 8 and 9 were obtained for the brain tissue shear modulus reported in the experiments by Miller and Chinzei (1997, 2002). Given a large variation of the brain tissue material properties reported and used in the literature, the generality of the results obtained for a single selected set of such properties may not be taken for granted. Therefore, we varied the brain tissue shear mod-
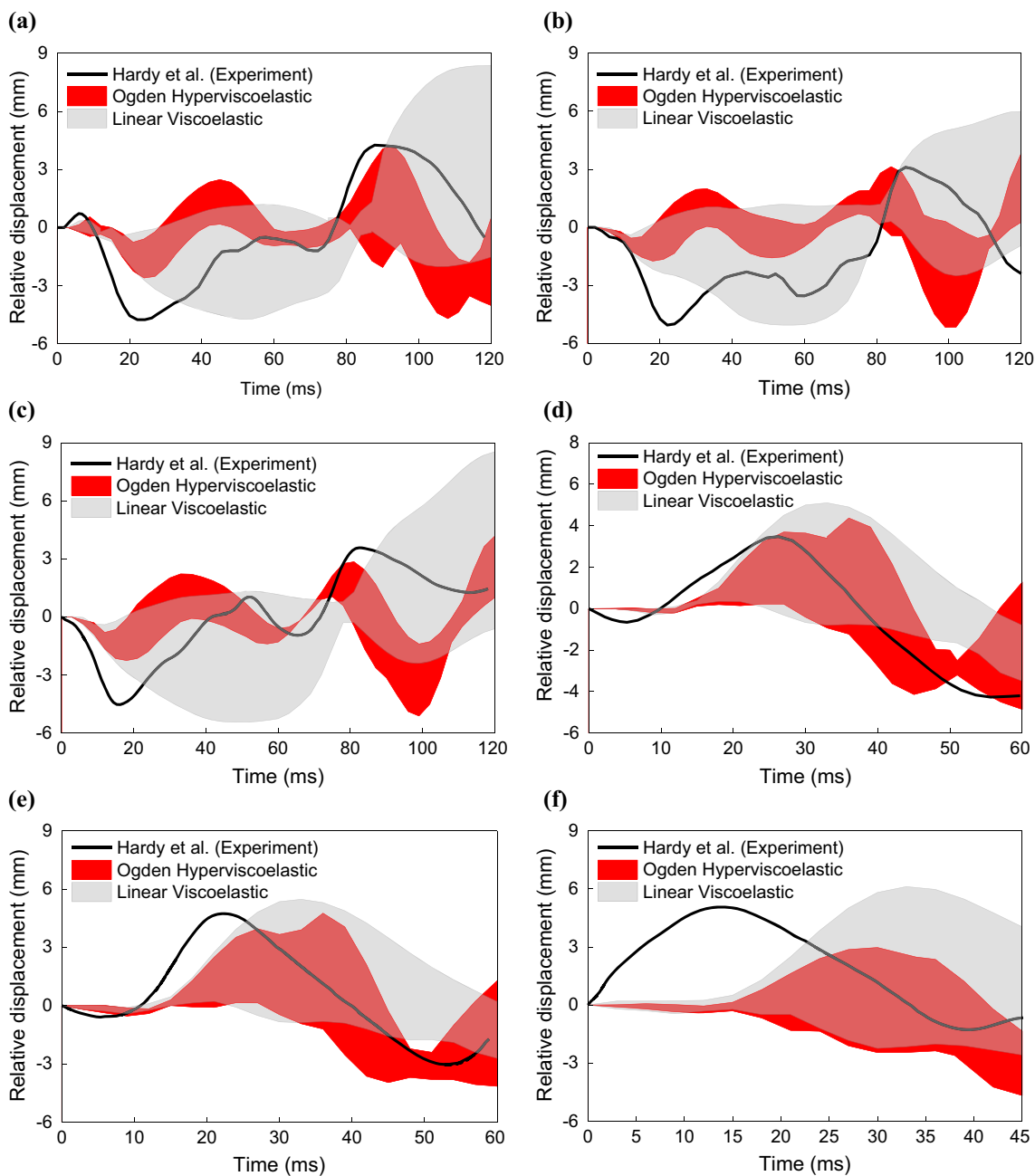
Fig. 8 Comparison of the predicted displacement time-history corridors (formed by four approaches for the brain–skull interface modelling, Table 2) of marker NDT #a1 in the sagittal plane for the linear viscoelastic (grey corridor) and Ogden hyperviscoelastic model (red corridor) constitutive models with the experimental results (black solid line) by Hardy et al. (2001). **a** Experiment C383-T1; **b** C383-T2; **c** C383-T3; **d** C755-T2; **e** C755-T3; **f** C755-T4. See Table 1 for information about the experiments by Hardy et al. (2001)

ulus following the data in Table 5. The results indicate that the NDT #a1 marker excursions (that are a measure of deformations within the brain) decrease when the instantaneous shear modulus of the grey matter and white matter increases and that for a given set of the white matter and grey matter shear modulus, the excursions predicted using the linear viscoelastic model are appreciably larger than for Ogden

hyperviscoelastic model (Fig. 10). These are intuitive and anticipated findings. The conclusions from analysis of the NDT #a1 marker trajectories shown in Fig. 9 are consistent with those when analysing the excursions. The magnitudes of the trajectories predicted for the material properties Sets 2, 3 and 4 (with shear modulus order of magnitude greater than in the base Set 1 derived from the experimental data by
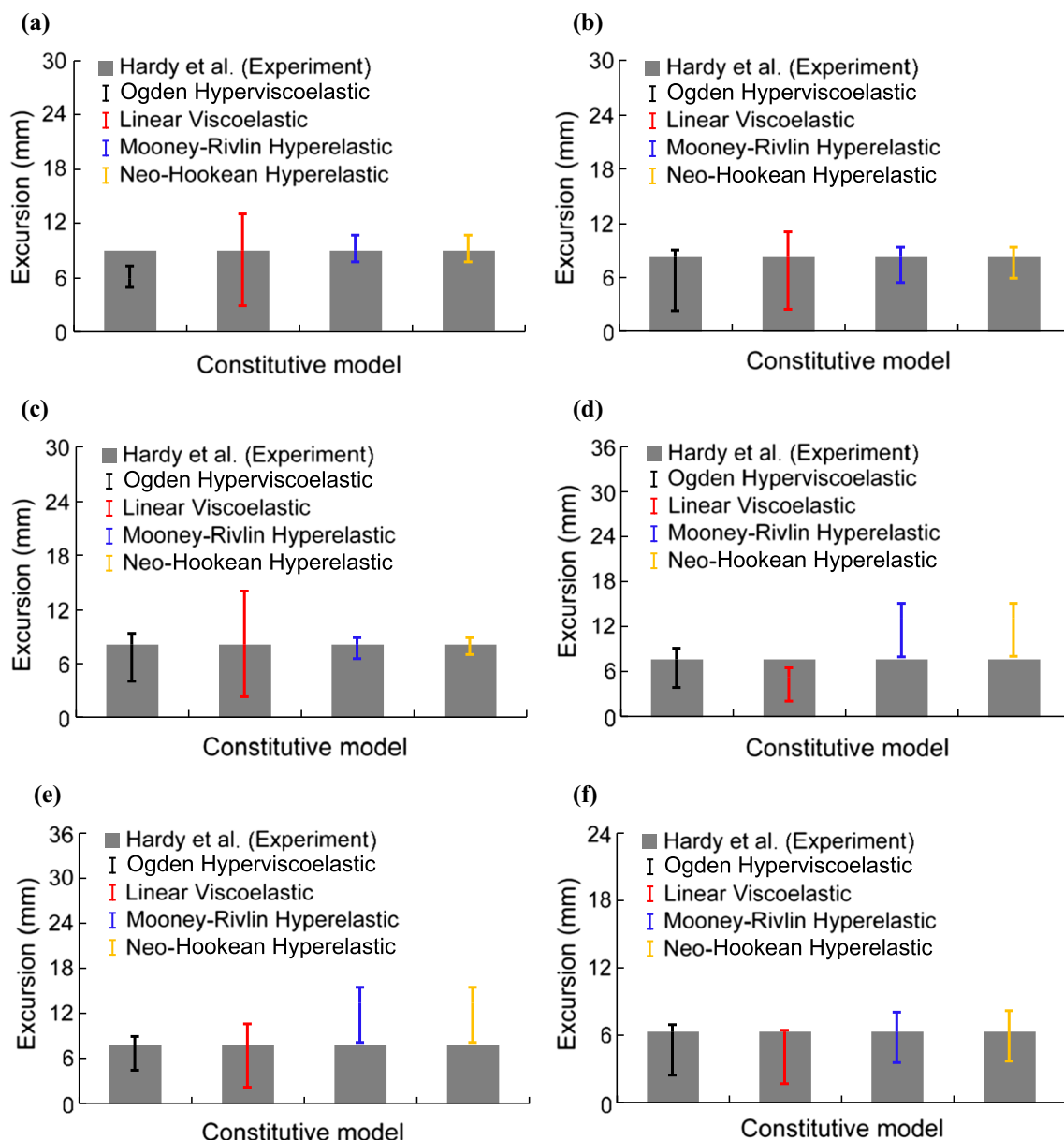
Fig. 9 Comparison of the magnitude envelopes (formed by four approaches for the brain–skull interface modelling summarised in Table 2) of the predicted excursions of NDT #a1 in the sagittal plane when using four types of the brain tissue constitutive model with the experimental results (grey bar) by Hardy et al. (2001). **a** Experiment C383-T1; **b** C383-T2; **c** C383-T3; **d** C755-T2; **e** C755-T3; **f** C755-T4. See Table 1 for the information about the experiments by Hardy et al. (2001)

Miller and Chinzei (1997, 2002), see Table 5) are appreciably smaller than those experimentally obtained by Hardy et al. (2001). Despite appreciable effects of the brain tissue properties on the NDT #a1 marker trajectory, the results in Fig. 11 are consistent with the observations made from Figs. 5, 6 and 7 when varying the approach for modelling the brain–skull interface. The predictions obtained using the approach for modelling the brain–skull interface used in THUMS model appear to be closer to the experimental data by Hardy et al. (2001) than the results for the remaining approaches summarised in Table 2.

3.2 Effects on the brain tissue strain and strain-based brain injury criteria

Comparison of the trajectories, time histories and displacement magnitudes of the selected points within the brain predicted by the computational biomechanics model and determined from the experiments by Hardy et al. (2001) (see Figs. 5, 6, 7, 8 and 9) provides information about the biofidelity of different approaches for modelling of the brain–skull interface and selection of constitutive model for the brain parenchyma tissues. However, from the perspective
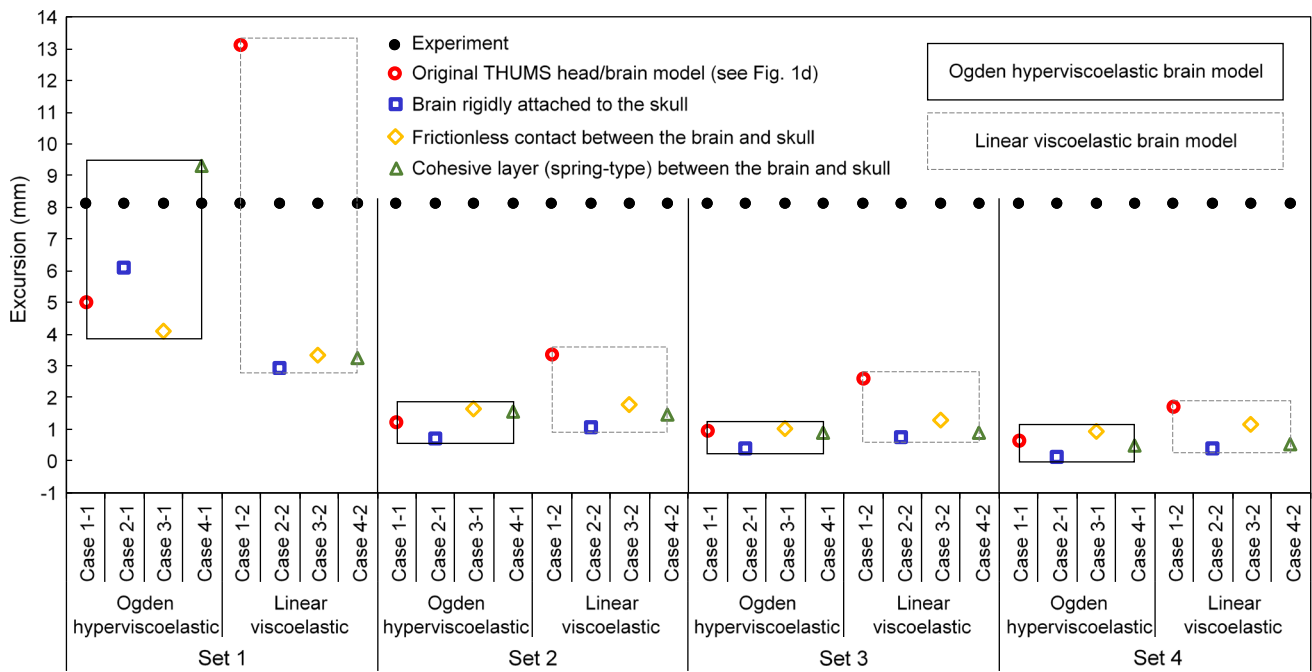
Fig. 10 Comparison of the predicted and observed [in the experiment C383-T3 by Hardy et al. (2001)] excursions of NDT #a1 marker located within the brain when varying the brain–skull interface modelling approach and brain tissue material properties (for Ogden hypervis-coelastic and linear viscoelastic constitutive model). Cases 1–1, 1–2, 2–1, 2–2, 3–1, 3–2, 4–1 and 4–2 refer to different approaches for modelling the brain–skull interface as defined in Table 2. The Sets 1, 2, 3 and 4 of materials properties are defined in Table 5

of application in injury analysis and prevention, the effects on the brain injury risk prediction are even more important. Analysis of these effects was conducted in two stages:

- *Stage 1* As many recently proposed brain injury criteria rely on information about the strain within the brain (Hernandez et al. 2015; Mao et al. 2006), we analysed the predicted maximum principal strain and maximum shear strain within the brain parenchyma. As prediction of the maximum strain values using models implemented using finite element method may be affected by localised phenomena/modelling artefacts, following Garlapati et al. (2014) and Wang et al. (2017), we used quantile plots of the maximum principal strain and shear strain at the time when the maximum strain value was observed.
- *Stage 2* We analysed the effects of approach for modelling of the brain–skull interface and constitutive model of the brain parenchyma on the cumulative strain damage measure (CSDM) brain injury criterion. We used the CSDM as it has been shown to be useful in evaluation of deformation-related brain impact injury (Bandak et al. 2001). Such injury is consistent with the impact severity in the experiments by Hardy et al. (2001). CSDM is defined as the volume fraction of the brain experiencing strain levels greater than a specified threshold (Bandak et al. 2001). Following the literature (Bandak et al. 2001;

Marjoux et al. 2008; Takhounts et al. 2008), we used a threshold of 0.15 and calculated the CSDM for the last time step of the simulation [i.e. at the end of the corresponding experiment by Hardy et al. (2001)].

Effects on the brain tissue strain Both the magnitude and distribution of the predicted strain were appreciably affected when varying the approach for modelling of the brain–skull interface and the brain parenchyma constitutive model (Fig. 12). For the maximum shear strain, the effect was of an order of magnitude (Fig. 12-right) while the predicted maximum principal strain changed by between 200 and 500% when varying the approach for modelling of the brain–skull interface and brain parenchyma constitutive model (Ogden hyperviscoelastic and linear viscoelastic) (Fig. 12-left).

Effects on the strain-based brain injury criteria The results indicate that the choices of the brain–skull interface and the constitutive model of the brain parenchyma are both important for calculation of the brain injury criteria (Fig. 13). Our results also show that an injury criterion relying solely on the maximum strain would lead to very different conclusions regarding the injury risk than the CSDM criterion that takes into account not only the strain magnitude, but also volume of the material subjected to the strain beyond a certain threshold (see Fig. 14; compare Figs. 12, 13).
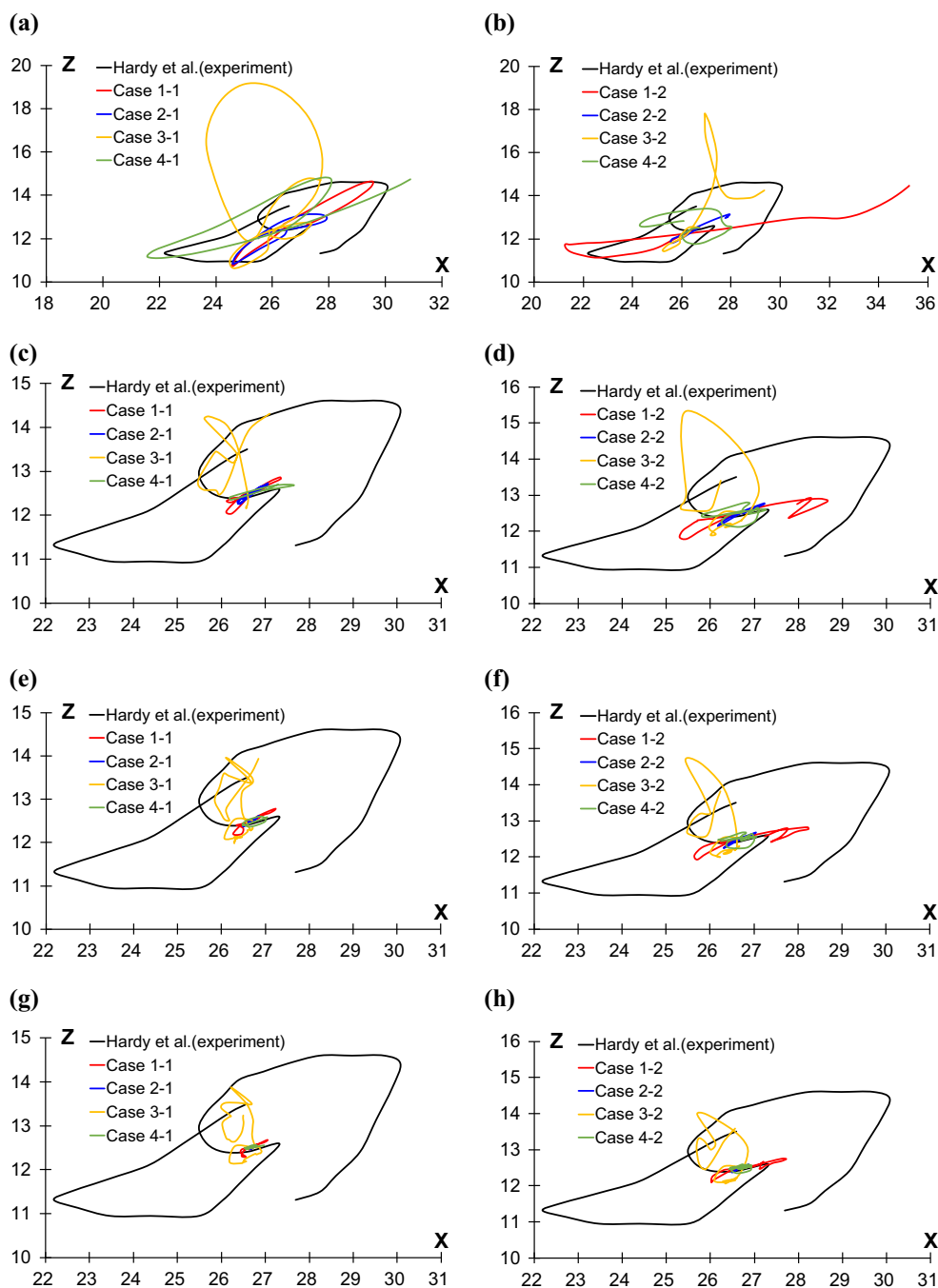
(a)

(b)

(c)

(d)

(e)

(f)

(g)

(h)

Fig. 11 Comparison of the predicted and observed [in the experiment C383-T3 by Hardy et al. (2001)] trajectories of NDT #a1 marker located within the brain when varying the brain–skull interface modelling approach and brain tissue material properties (for Ogden hyperviscoelastic and linear viscoelastic constitutive models). **a** Ogden hyperviscoelastic model for the brain tissue with Set 1 of the material properties; **b** linear viscoelastic model of the brain tissue with Set 1 of the material properties; **c** Ogden hyperviscoelastic model of the brain tissue with Set 2 of the material properties; **d** Linear viscoelastic model of the brain tissue with Set 2 of the material properties; **e** Ogden hyperviscoelastic model of the brain tissue with Set 3 of the material properties; **f** linear viscoelastic model of the brain tissue with Set 2 of the material properties; **g** Ogden hyperviscoelastic model of the brain tissue with Set 4 of the material properties; **h** Linear viscoelastic model of the brain tissue with Set 4 of the material properties. Cases 1–1, 1–2, 2–1, 2–2, 3–1, 3–2, 4–1 and 4–2 refer to different approaches for modelling the brain–skull interface as defined in Table 2. The Sets 1, 2, 3 and 4 of material properties are defined in Table 5
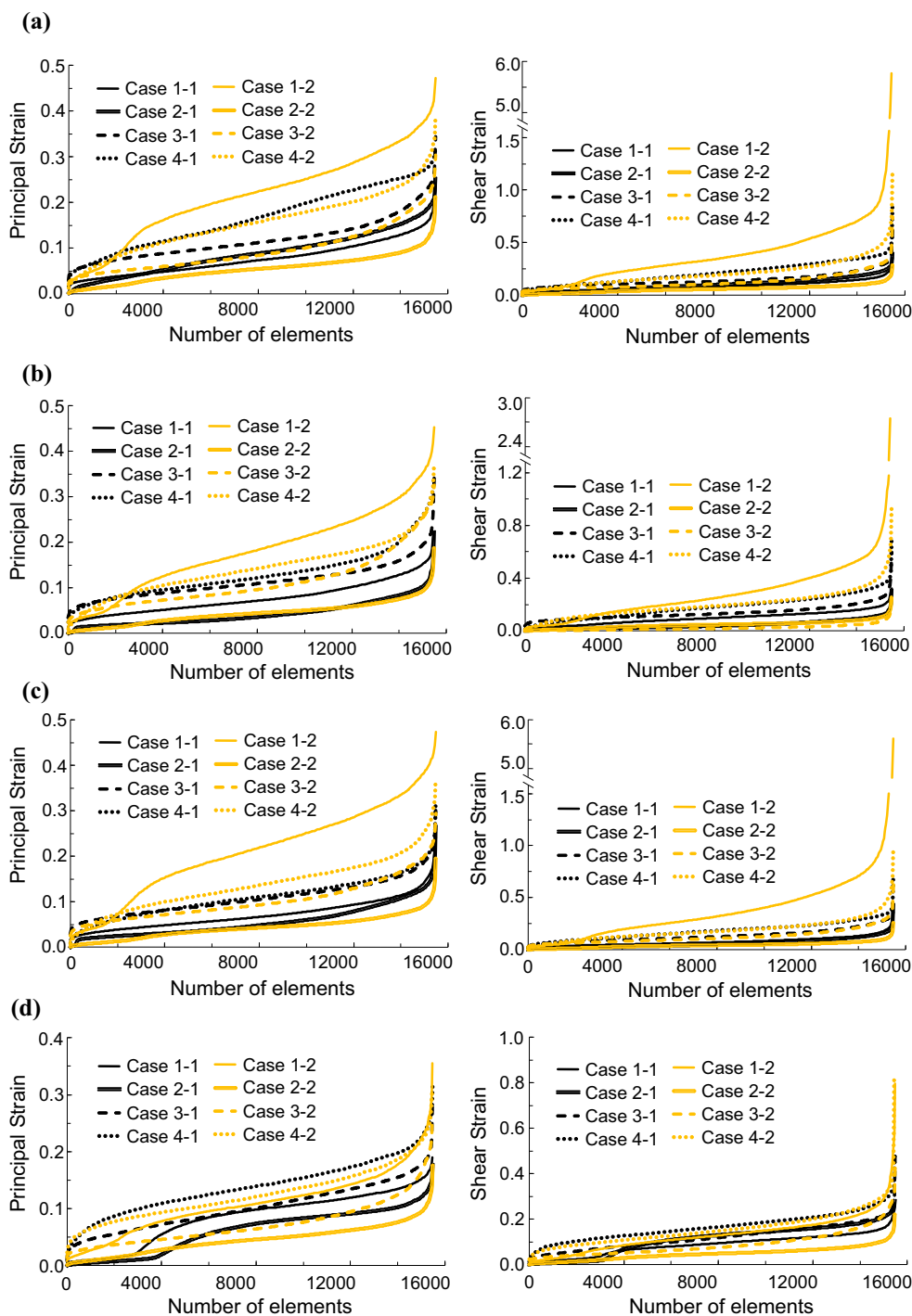
Fig. 12 Quantile plots of principal (left) and shear (right) strain (Almansi) when varying brain–skull interface modelling approach and constitutive model for the brain parenchyma tissue when modelling the experiments by Hardy et al. (2001). **a** Experiment C383-T1; **b** C383-T2; **c** C383-T3; **d** C755-T2; **e** C755-T3; **f** C755-T4. Cases 1–1 and 1–2: original approach used in THUMS Version 4.0 model with direct representation of the CSF and brain meninges; Cases 2–1 and 2–2: brain rigidly attached to the skull; Cases 3–1 and 3–2: frictionless sliding contact between the brain and skull; Cases 4–1 and 4–2: brain–skull interface modelled using a layer of spring-type cohesive elements. Cases 1–1, 2–1, 3–1 and 4–1: Ogden hyperviscoelastic model for the brain parenchyma tissue; Cases 1–1, 2–1, 3–1 and 4–1: linear viscoelastic model for the brain parenchyma tissue. Description of the experiments by Hardy et al. (2001) is in Table 1. The simulation matrix is in Table 2
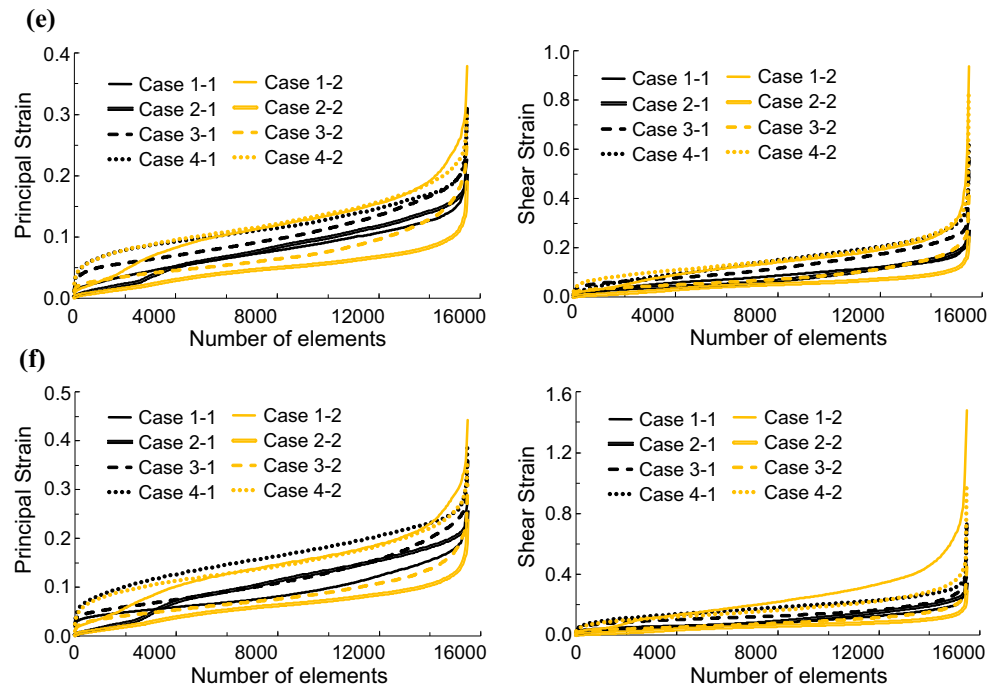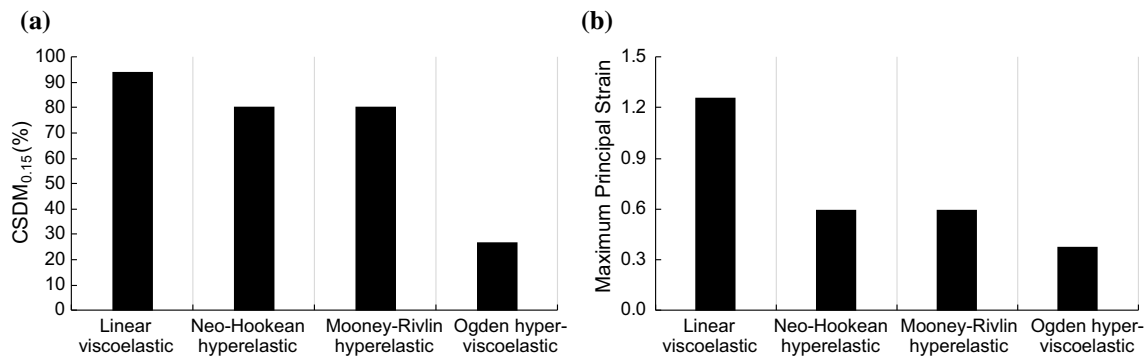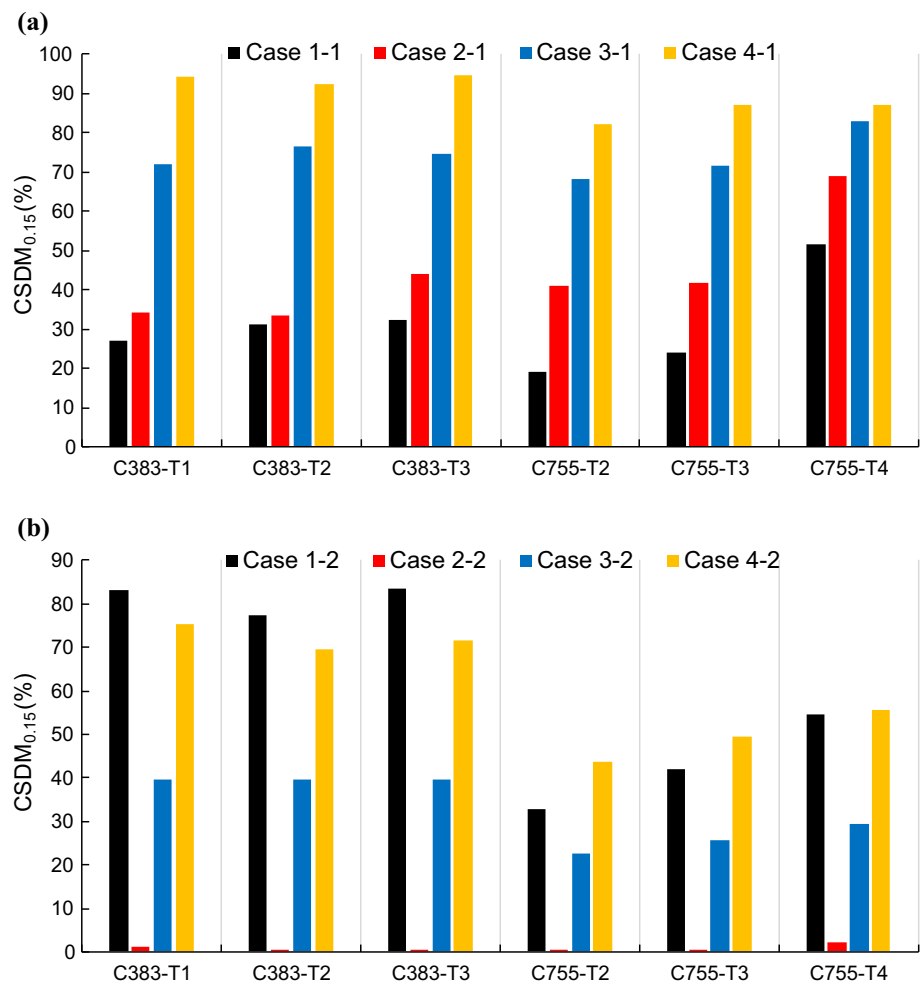
Fig. 12 continued

4 Discussion

4.1 Effects of modelling choice for the brain–skull interface

Our study indicates that the kinematics of the selected points (Figs. 6, 7 and 8) and strain (Fig. 12) within the brain predicted using a computational biomechanics model are appreciably affected by the approach for modelling of the brain–skull interface employed in the model. This result is consistent with the studies by Kleiven and Hardy (2002), Wittek and Omori (2003) and Wang et al. (2017).

The approach for the brain–skull interface modelling taken from THUMS model, that includes direct representation of the subarachnoidal space with CSF, appears to result in the smallest differences with the experimental results by Hardy et al. (2001), with the excursions of the selected points within the brain close to those reported by Hardy et al. (2001) (Figs. 7, 9 and Table 6). This approach allows for relative movement between the brain and skull, while preventing separation/detachment between them (Fig. 15a) and is consistent with the anatomical structure of brain–skull interface according to Haines et al. (1993). The approach using cohesive elements (that can be regarded as a three-dimensional spring and damper, with three stiffness and three damping constants) also allows for such movement and prevents the brain–skull separation/detachment (Fig. 15d). We derived the stiffness of the cohesive elements from the study by Mazumder et al. (2013) conducted under loads compatible with neurosurgery

in direction tangential to the skull. Consequently, the results by Mazumder et al. (2013) contain very limited information about the brain–skull interface stiffness in direction normal to the skull, which limits the biofidelity of our approach for modelling the brain–skull interface using cohesive elements.

For some experiments by Hardy et al. (2001), the predictions obtained using the approach with the brain rigidly attached/tied to the skull resulted in marginally better agreement (given up to 0.46 mm standard deviation when determining the brain deformation in these experiments) with the experimental data by Hardy et al. (2001) than the approach with direct representation of the CSF (Table 6, Fig. 7a, e). However, as the approach using the brain rigidly attached/tied to the skull is not supported by the brain–skull interface anatomy (Fig. 1) and, in particular, allows no relative movement between the brain and skull (Fig. 15b), any recommendations regarding application of this approach in prediction of brain deformations and risk of brain injury should be made very carefully and require further studies.

Frictionless contact between the brain and skull (that allows for unconstrained movement between the brain and skull in direction tangential to the skull and complete separation between the brain and skull) (Fig. 15c) resulted in large discrepancies between the predictions and experiments by Hardy et al. (2001) (Figs. 7, 8 and 9).

Fig. 14 Comparison of CSDM (**a**) and maximum principal strain (**b**) brain injury criteria predicted using THUMS Version 4.0 model when modelling the experiment C383-T1 by Hardy et al. (2001) using Ogden hyperviscoelastic model, Mooney–Rivlin hyperelastic model, neo-Hookean hyperelastic model and linear viscoelastic model for the parenchyma tissue. Brain–skull interface from original THUMS 4.0 model with direct representation of the CSF and brain meninges was used (see Fig. 2)

4.2 Effects of constitutive model of the brain tissue

Our study indicates that application of Ogden hyperviscoelastic model to represent the constitutive behaviour of grey matter and white matter leads to much better agreement with the experimental results by Hardy et al. (2001) than the Mooney–Rivlin hyperelastic, neo-Hookean hyperelastic, and, in particular, linear viscoelastic models. The linear viscoelastic model tends to appreciably overestimate the brain deformations as determined from the motion of the selected points within the brain (Figs. 8, 9). This can be explained by the fact that for the Ogden model, we used the mate-
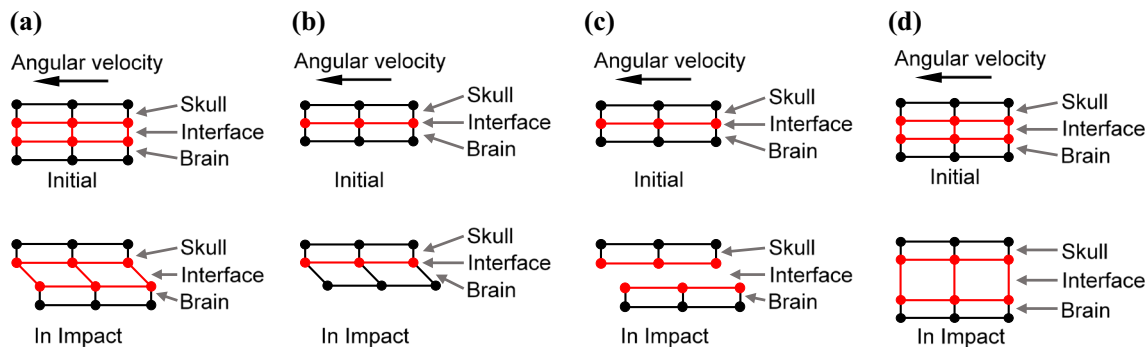
Fig. 15 Schematic representation of predicted brain deformations and relative motion between the brain and skull for different approaches for the brain–skull interface modelling. **a** Original approach used in THUMS Version 4.0 model with direct representation of the CSF and brain meninges (Fig. 1d); **b** brain rigidly attached to the skull; **c** frictionless sliding contact between the brain and skull; **d** brain–skull interface modelled using a layer of spring-type cohesive elements

rial coefficient $\alpha = -4.7$ (a value taken from Miller and Chinzei 2002, see Eq. 1) which leads to strongly nonlinear stress–strain relationship and significant increase of the tissue stiffness (in compression) at large strain. For the neo-Hookean constitutive model, the material coefficient $\alpha = 2$ and the nonlinearity of the stress–strain relationship is less pronounced than for the Ogden model. This explanation is consistent with the fact that appreciably larger strain within the brain tissue was predicted for linear viscoelastic and neo-Hookean constitutive model of the brain tissue than for the Ogden model (Fig. 12), and the differences between the strain predicted using Ogden model and the remaining constitutive models used in this study increased with the impact severity (Fig. 12a-right, b-right, c-right and Table 1).

From the perspective of injury analysis and prevention, the effects on the brain injury criteria rather than on the brain deformations and strain induced by violent impact are more important. Therefore, we analysed the effects of the constitutive model of the brain parenchyma on cumulative strain damage measure (CSDM) and maximum principal strain (MPS) strain-based injury criteria. Appreciably lower CSDM and MPS were obtained for Ogden hyperviscoelastic model than for neo-Hookean hyperelastic and linear viscoelastic constitutive models (Fig. 14).

4.3 Effects of constitutive properties of the brain tissue

Although varying the constitutive properties (shear modulus) of the brain tissue exerted appreciable effects on the predicted deformations within the brain (as measured by the excursions and trajectories of the selected points located within the brain), the results are intuitive and anticipated. The deformations decreased when the shear modulus of the grey matter and white matter increased (Figs. 10, 11). This finding does not affect the conclusions regarding the approach for mod-

elling the brain–skull interface. For all values of the grey matter and white matter shear modulus used in this study, the results obtained using the approach for modelling the brain–skull interface from the THUMS model appear to be closer to the experimental data by Hardy et al. (2001) than the predictions made using the remaining approaches summarised in Table 2. The results presented in Fig. 10 raise the possibility of increasing the shear modulus of linear viscoelastic model, from 800 Pa based on the experiments by Miller and Chinzei (1997, 2002), so that the predicted brain deformations are as close to the experimental data by Hardy et al. (2001) as when using Ogden hyperviscoelastic model. However, such calibration would imply that the validation comparison is calibrated to the validation data. Therefore, we have not attempted to calibrate the material properties to the brain deformations measured by Hardy et al. (2001).

4.4 Limitations

The limitations of the methods used in this paper stem from a number of sources. The primary limitation lays in the experimental results of Hardy et al. (2001) and Hardy (2007) we used for comparison with our numerical studies. One of the key limitations of Hardy's experiments using PMHSs is that they do not provide injury responses. Consequently, although we also investigated the effects on prediction of brain injury using strain-based injury criteria (cumulative strain damage measure, maximum principal strain, and maximum shear strain), no experimental data to evaluate these predictions are available. Therefore, in this study, we do not formulate any conclusions regarding biofidelity of different brain injury criteria. Nevertheless, in our opinion, Hardy's experiments provide the best data currently available and our choice of using these data for comparisons is justified.

Another limitation of this study is the use of generic head geometry rather than subject-specific one. Unfortunately,

Hardy et al. (2001) and Hardy (2007) have not collected MRI and CT images of their experimental subjects, and therefore, exact geometries of the heads and brains in used in their experiments are unknown. As methods for constructing subject-specific models rely on such images (Wittek et al. 2016), we could not quantify the effects of subject-specific geometry in this study.

Another limitation of our study, common to practically all published work in brain injury biomechanics, is an exclusion of fluid-structure interaction in the model.

One also needs to remember the inherent difficulties with conducting very comprehensive computer simulations with the finite element method, including possible, but difficult to quantify, effects of hourglass control mechanism.

5 Conclusions

(1) When applying computational biomechanics models to predict deformations within the brain due to violent impact in sagittal plane, the results are strongly affected by both the modelling choice for the brain–skull interface and constitutive model of the brain parenchyma. Our quantitative analysis here indicates that the predicted deformations may be more sensitive to changing the brain tissue constitutive model from Ogden hyperviscoelastic to linear viscoelastic than to varying the approach for modelling of the brain–skull interface between two extreme choices: the brain outer surface rigidly attached to the skull and frictionless contact between the brain and skull. However, the current study clearly shows that focusing either on the constitutive model of the brain tissue or modelling of the conditions brain–skull interface (that determines boundary conditions for the brain) alone does not guarantee accurate prediction of the brain responses under violent impact. Although this conclusion is consistent with the commonly accepted guidelines regarding formulation of computational biomechanics models (Bathe 2006), investigation of boundary conditions attracted much less attention of the biomechanics research community than constitutive behaviour of soft tissues (Agrawal et al. 2015).

(2) For the four approaches for modelling the brain–skull interface analysed here (subarachnoidal space and cerebrospinal fluid directly represented in the model, brain outer surface rigidly attached to the skull, frictionless contact between the brain and skull, brain–skull interface represented using a layer of cohesive elements), the one with direct representation of the subarachnoidal space and cerebrospinal fluid (approach originally used in THUMS Version 4.0 model) appears to result in better agreement between the modelling predictions and experimental results by Hardy et al. (2001) than the remaining approaches. This may not necessarily indicate inadequacy of the approach using cohesive elements, but underscores the gap in the knowledge of the mechanical properties of the brain–skull interface.

(3) Prediction of deformations within the brain due to violent impact using computational biomechanics models requires accurate representation of nonlinear stress–strain relationship of the brain tissue. The current study suggests that such prediction can be achieved using Ogden hyperviscoelastic constitutive model. It also indicates that application of linear viscoelastic model may lead to overestimation of deformations within the brain and, consequently, overestimation of injury risk if strain-based injury criteria are used. To the best of our knowledge, such observations and suggestions regarding the brain tissue constitutive model have not been previously made.

Compliance with ethical standards

Conflict of interest Adam Wittek was employed by Toyota Central Research and Development Laboratories in 2002–2004, where he was involved in development of the brain model for Total HUman Model for Safety (THUMS). He is a co-author of patent (in Japan) 2004-303220 "Method for determining brain damage, and human head finite element model" by Toyota Central and Development Laboratories.

References

Agrawal S, Wittek A, Joldes G, Bunt S, Miller K (2015) Mechanical properties of brain-skull interface in compression. In: Doyle B, Miller K, Wittek A, Nielsen PMF (eds) Computational biomechanics for medicine. Springer, New York, pp 83–91. https://doi.org/10.1007/978-3-319-15503-6_8

Al-Bsharat AS, Hardy WN, Yang KH, Khalil TB, Tashman S, King AI (1999) Brain/skull relative displacement magnitude due to blunt head impact. In: Proceedings of the 1999 43rd stapp car crash conference, San Diego, CA, USA. SAE, Warrendale, PA, U.S.A, pp 321–332

Almeida CERd, Filho JLdS, Dourado JC, Gontijo PAM, Dellaretti MA, Costa BS (2016) Traumatic brain injury epidemiology in Brazil. World Neurosurg 87:540–547 10.1016/j.wneu.2015.10.020

Antona-Makoshi J (2013) Reanalysis of primate head impact experiments to clarify mild traumatic brain injury kinematics and thresholds. Dissertation, Chalmers University of Technology

Antona-Makoshi J (2015) Traumatic brain injuries: animal experiments and numerical simulations to support the development of a brain injury criterion. Dissertation, Chalmers University of Technology

Bandak FA, Zhang AX, Tannous RE, DiMasi F, Masiello P, Eppinger R (2001) SIMon: a simulated injury monitor; application to head injury assessment. In: International technical conference on the enhanced safety of vehicles, Amsterdam, The Netherlands. National Highway Traffic Safety Administration, p 7

Bathe K-J (2006) Finite element procedures. Prentice Hall, Upper Saddle River

Bayly PV, Clayton EH, Genin GM (2012) Quantitative imaging methods for the development and validation of brain biomechanics models. Annu Rev Biomed Eng 14:369–396 10.1146/annurev-bioeng-071811-150032

Bilston LE (2011) Brain tissue mechanical properties. Stud Mechanobiol Tissue Eng Biomater 3:69–89 10.1007/978-1-4419-9997-9_4

Claessens M, Sauren F, Wismans J (1997) Modeling of the human head under impact conditions: a parametric study. SAE Technical Paper: No. 973338. https://doi.org/10.4271/973338

Fahlstedt M, Halldin P, Alvarez VS, Kleiven S (2016) Influence of the body and neck on head kinematics and brain injury risk in bicycle accident situations. In: Proceedings of 2016 IRCOBI conference. International research council on biomechanics of injury (IRCOBI), Malaga, Spain, pp 459–478

Faul M, Xu L, Wald MM, Coronado V (2010) Traumatic brain injury in the United States: emergency department visits, hospitalizations and deaths 2002–2006 (blue book). National Center for Injury Prevention and Control, Centers for Disease Control and Prevention, Atlanta

Feng Y, Abney T, Okamoto R, Pless R, Genin G, Bayly PV (2010) Relative brain displacement and deformation during constrained mild frontal head impact. J R Soc Interface 7:1677–1688 10.1098/rsif.2010.0210

Garlapati R et al (2014) More accurate neuronavigation data provided by biomechanical modeling instead of rigid registration. J Neurosurg 120:1477–1483 10.3171/2013.12.JNS131165

Haines DE, Harkey HL, Al-Mefty O (1993) The "subdural" space: a new look at an outdated concept. Neurosurgery 32:111–120 10.1227/00006123-199301000-00017

Hardy WN (2007) Response of the human cadaver head to impact. Dissertation, Wayne State University

Hardy WN, Foster CD, Mason MJ, Yang KH, King AI, Tashman S (2001) Investigation of head injury mechanisms using neutral density technology and high-speed biplanar x-ray. Stapp Car Crash J 45:337–368

Hernandez F et al (2015) Six degree-of-freedom measurements of human mild traumatic brain injury. Ann Biomed Eng 43:1918–1934 10.1007/s10439-015-1487-0

Ho J, Kleiven S (2007) Dynamic response of the brain with vasculature: a three-dimensional computational study. J Biomech 40:3006–3012 10.1016/j.jbiomech.2007.02.011

Hu J et al (2007) Intraoperative brain shift prediction using a 3D inhomogeneous patient-specific finite element model. J Neurosurg 106:164–169 10.3171/jns.2007.106.1.164

Iwamoto M, Nakahira Y, Kimpara H (2015) Development and validation of the total human model for safety (THUMS) toward further understanding of occupant injury mechanisms in pre-crash and during crash. Traffic Inj Prev 16(Suppl 1):S36 10.1080/15389588.2015.1015000

Jin X (2009) Biomechanical response and constitutive modeling of bovine pia-arachnoid complex. Dissertation, Wayne State University

Jin X, Yang KH, King AI (2011) Mechanical properties of bovine pia-arachnoid complex in shear. J Biomech 44:467–474 10.1016/j.jbiomech.2010.09.035

Jin X, Mao H, Yang KH, King AI (2014) Constitutive modeling of pia-arachnoid complex. Ann Biomed Eng 42:812–821 10.1007/s10439-013-0948-6

Kimpara H, Nakahira Y, Iwamoto M, Miki K, Ichihara K, Kawano S, Taguchi T (2006) Investigation of anteroposterior head-neck responses during severe frontal impacts using a brain-spinal cord complex FE model. Stapp Car Crash J 50:509–544

Kleiven S, Hardy WN (2002) Correlation of an FE model of the human head with local brain motion: consequences for injury prediction. Stapp Car Crash J 46:123–144

LSTC (2007) LS-DYNA keyword user's manual, version 971. Livermore Software Technology Corporation Livermore, United States of America

Mao H et al (2013) Development of a finite element human head model partially validated with thirty five experimental cases. J Biomech Eng 135:111002 10.1115/1.4025101

Mao H, Zhang L, Yang KH, King AI (2006) Application of a finite element model of the brain to study traumatic brain injury mechanisms in the rat. Stapp Car Crash J 50:583–600

Marjoux D, Baumgartner D, Deck C, Willinger R (2008) Head injury prediction capability of the HIC, HIP, SIMon and ULP criteria. Accid Anal Prev 40:1135–1148 10.1016/j.aap.2007.12.006

Mazumder MMG et al (2013) Mechanical properties of the brain-skull interface. Acta Bioeng Biomech 15:9 10.5277/abb130201

McElhaney JH, Melvin JW, Roberts VL, Portnoy HD (1973) Dynamic characteristics of the tissues of the head. Palgrave Macmillan, Basingstoke

Mihai LA, Chin LK, Janmey PA, Goriely A (2015) A comparison of hyperelastic constitutive models applicable to brain and fat tissues. J R Soc Interface 12:20150486 10.1098/rsif.2015.0486

Miller K (2011) Biomechanics of the brain. Springer, New York 10.1007/978-1-4419-9997-9

Miller K, Chinzei K (1997) Constitutive modelling of brain tissue: experiment and theory. J Biomech 30:1115–1121. https://doi.org/10.1016/S0021-9290(97)00092-4

Miller K, Chinzei K (2002) Mechanical properties of brain tissue in tension. J Biomech 35:483–490 10.1016/S0021-9290(01)00234-2

Miller RT, Margulies SS, Leoni M, Nonaka M, Chen X, Smith DH, Meaney DF (1998) Finite element modeling approaches for predicting injury in an experimental model of severe diffuse axonal injury. SAE Technical Paper: 983154. https://doi.org/10.4271/983154

Miller K, Chinzei K, Orssengo G, Bednarz P (2000) Mechanical properties of brain tissue in-vivo: experiment and computer simulation. J Biomech 33:1369–1376 10.1016/S0021-9290(00)00120-2

Miller K, Wittek A, Joldes G, Horton A, Dutta-Roy T, Berger J, Morriss L (2010) Modelling brain deformations for computer-integrated neurosurgery. Int J Numer Methods Biomed 26:117–138 10.1002/cnm.1260

Miller K, Wittek A, Joldes G (2011) Biomechanical modeling of the brain for computer-assisted neurosurgery. Biomechanics of the brain. Springer, New York

NHTSA (2010) Federal motor vehicle safety standards: occupant crash protection. National Highway Traffic Safety Administration, USA

Ogden RW (1997) Non-linear elastic deformations. Dover Publications, New York

Peeters W, Brande RVD, Polinder S, Brazinova A, Steyerberg EW, Lingsma HF, Maas AIR (2015) Epidemiology of traumatic brain injury in Europe. Acta Neurochir 157:1683–1696 10.1007/s00701-015-2512-7

Rashid B, Destrade M, Gilchrist MD (2013) Mechanical characterization of brain tissue in simple shear at dynamic strain rates. J Mech Behav Biomed 28:71–85 10.1016/j.jmbbm.2013.07.017

Shigeta K, Kitagawa Y, Yasuki T (2009) Development of next generation human FE model capable of organ injury prediction. In: International technical conference on the enhanced safety of vehicles (ESV). Germany. National Highway Traffic Safety Administration, Stuttgart, pp 09–0111

Takhounts EG, Eppinger RH, Campbell JQ, Tannous RE, Power ED, Shook LS (2003) On the development of the SIMon finite element head model. Stapp Car Crash J 47:107–133

Takhounts EG et al (2008) Investigation of traumatic brain injuries using the next generation of simulated injury monitor (SIMon) finite element head model. Stapp Car Crash J 52:1–31

Takhounts EG, Craig MJ, Moorhouse K, McFadden J, Hasija V (2013) Development of brain injury criteria (Br IC). Stapp Car Crash J 57:243–266

Wang F, Geng Z, Agrawal S, Han Y, Miller K, Wittek A (2017) Computation of brain deformations due to violent impact: quantitative analysis of the importance of the choice of boundary conditions and brain tissue constitutive model. In: Wittek A, Joldes G, Nielsen PMF, Doyle BJ, Miller K (eds) Computational biomechanics for medicine. Springer, New York, pp 159–173

Watanabe R, Miyazaki H, Kitagawa Y, Yasuki T (2011) Research of collision speed dependency of pedestrian head and chest injuries using human FE model (THUMS version 4). In: Proceedings of 22nd enhanced safety of vehicles (ESV) conference, Washington DC, USA. National Highway Traffic Safety Administration, pp 11-0043

Wittek A, Omori K (2003) Parametric study of effects of brain-skull boundary conditions and brain material properties on responses of simplified finite element brain model under angular acceleration in sagittal plane. JSME Int J 46:1388–1398 10.1299/jsmec.46.1388

Wittek A, Miller K, Kikinis R, Warfield SK (2007) Patient-specific model of brain deformation: application to medical image registration. J Biomech 40:919–929 10.1016/j.jbiomech.2006.02.021

Wittek A, Dutta-Roy T, Taylor Z, Horton A, Washio T, Chinzei K, Miller K (2008) Subject-specific non-linear biomechanical model of needle insertion into brain. Comput Methods Biomed 11:135–146 10.1080/10255840701688095

Wittek A, Joldes G, Couton M, Warfield SK, Miller K (2010) Patient-specific non-linear finite element modelling for predicting soft organ deformation in real-time: application to non-rigid neuroimage registration. Prog Biophys Mol Biol 103:292–303 10.1016/j.pbiomolbio.2010.09.001

Wittek A, Grosland NM, Joldes GR, Magnotta V, Miller K (2016) From finite element meshes to clouds of points: a review of methods for generation of computational biomechanics models for patient-specific applications. Ann Biomed Eng 44:3–15 10.1007/s10439-015-1469-2

Yang J (2011) Investigation of brain trauma biomechanics in vehicle traffic accidents using human body computational models. In: Wittek A, Nielsen PMF, Miller K (eds) Computational biomechanics for medicine. Springer, New York, pp 5–14 10.1007/978-1-4419-9619-0_2

Yang KH, King AI (2011) Modeling of the brain for injury simulation and prevention. In: Miller K (ed) Biomechanics of the brain. Springer, New York, pp 90–110 10.1007/978-1-4419-9997-9_5

Yang J, Xu W, Otte D (2008) Brain injury biomechanics in real world vehicle accident using mathematical models. Chin J Mech Eng EN 32:81–86 10.3901/CJME.2008.04.081

Zhang L et al (2001) Recent advances in brain injury research: a new human head model development and validation. Stapp Car Crash J 45:369–394